

A Comparative Study of Structural and Ethanol Gas Sensing Properties of Pure, Nickel and Palladium Doped SnO₂ Nanorods Synthesised by the Hydrothermal Method

Vicinisvarri Inderan,^{1,2} M. M. Arafat,³ A. S. M. A. Haseeb,³ Kumar Sudesh⁴ and Hooi Ling Lee^{1*}

¹Nanomaterials Research Group, School of Chemical Sciences, Universiti Sains Malaysia, 11800 USM Pulau Pinang, Malaysia

²Department of Applied Sciences, Universiti Teknologi MARA, Cawangan Pulau Pinang, Jalan Permatang Pauh, 13500 Permatang Pauh, Pulau Pinang, Malaysia

³Department of Mechanical Engineering, Faculty of Engineering, University of Malaya, 50603 Kuala Lumpur, Malaysia

⁴School of Biological Sciences, Universiti Sains Malaysia, 11800 USM Pulau Pinang, Malaysia

*Corresponding author: hllee@usm.my

Published online: 25 April 2019

To cite this article: Inderan, V. et al. (2019). A comparative study of structural and ethanol gas sensing properties of pure, nickel and palladium doped SnO₂ nanorods synthesised by the hydrothermal method. *J. Phys. Sci.*, 30(1), 127–143, <https://doi.org/10.21315/jps2019.30.1.10>

To link to this article: <https://doi.org/10.21315/jps2019.30.1.10>

ABSTRACT: SnO₂ nanostructures are usually modified with some metal dopants in order to improve its gas sensing properties. In this work, pure tin oxide (SnO₂), nickel (Ni) doped SnO₂ (Ni:SnO₂) and palladium (Pd) doped SnO₂ (Pd:SnO₂) nanorods were successfully synthesised via hydrothermal method at low temperature (180°C) without templates or further calcination. All the samples were systematically analysed using X-ray powder diffraction (XRD), X-ray photoelectron spectroscopy (XPS), field emission scanning electron microscopy (FESEM) and high resolution transmission electron microscopy (HRTEM). The sensor response ($R = R_0/R_g$) towards 1000 ppm ethanol gas was investigated using nitrogen gas as a carrier gas. XRD results confirmed that all samples consisted of rutile tetragonal-shaped SnO₂. It was found that the average diameter of nanorods formed in Ni:SnO₂ and Pd:SnO₂ were decreased to ~6 nm and ~10 nm, compared with nanorods formed in pure SnO₂ (~25 nm). The gas sensing results indicated that the sensor properties of SnO₂ were enhanced after the doping process. At 450°C, the Pd:SnO₂ nanorod sensor recorded the highest response value towards 1000 ppm ethanol gas which is 15 times higher than pure SnO₂ nanorods. Interestingly, all samples showed similar response time, ~ 40 s. However, pure SnO₂ and Ni:SnO₂ nanorods sensors exhibited longer recovery

time compared to Pd:SnO₂ nanorods. Pd:SnO₂ nanorods recorded only 12 min of almost 100% recovery. It is proposed that Pd:SnO₂ sensor could be a promising candidate for the detection of ethanol gas.

Keywords: Hydrothermal, Pd doped, Ni doped, tin oxide, nanorods, gas sensor

1. INTRODUCTION

The application of metal oxide as a gas sensor has attracted many researchers' attention ever since Seiyama et al. discovered that the adsorption and desorption of gases on the surface of zinc oxide (ZnO) films caused rapid changes in electrical conductivity.¹ Since then, various types of metal oxides have been extensively studied for the detection of a wide variety of air pollutants, toxic, combustible and process gases. Among them, one-dimensional (1-D) tin oxide (SnO₂) nanostructures as a gas sensor has great advantages such as high sensitivity towards various reducing and oxidising gases, large surface-to-volume ratio, low cost and compatibility with microfabrication.^{2,3} Nevertheless, the sensing properties of pure SnO₂ still needs to be further improved due to their poor sensitivity, selectivity and lengthy recovery time.⁴ To overcome these disadvantages, an efficient method is the doping of SnO₂ with transition or noble metals.⁵ The fundamental theory of doping is to enhance its catalytic activity and modify its electric resistance for the gas sensor.⁶

Several studies have been reported on noble metals-doped (e.g., Pt, Pd, Ag, Au, etc.) SnO₂ sensors.⁷⁻⁹ These sensors are sensitive to a wide number of toxic and explosive gases including ethanol gas. Among them, Pt and Pd are the most commonly used dopants in enhancing the sensing properties of SnO₂, owing to their high oxidation catalytic properties. For instance, Lee et al. reported that Pd-doped SnO₂ nanorod thin films prepared by plasma-enhanced chemical vapour deposition (PECVD) method showed 2.5 times higher sensor response with full recovery towards 1000 ppm ethanol gas at 300°C compared to un-doped SnO₂.¹⁰ It was suggested that changes in the oxidation state of Pd was the key factor that promoted the gas sensing properties of Pd-doped SnO₂. Meanwhile, Ivanov et al. fabricated an ethanol gas sensor using Pt-doped SnO₂ where the detection limit was at sub-ppb level and with high sensitivity and fast response.¹¹

In contrast, transition metal dopants such as Ni, Co and Fe are well known for crystal growth inhibitors.¹²⁻¹⁴ Wu et al., in a study, explained that the interaction on the boundaries between the host and dopant crystallites resisted the motion of crystallites and stunted crystal growth.¹⁵ As a result, the size of crystallites was decreased by the doping process. Besides that, the incorporation of transitional

metal doping also increased oxygen vacancies and subsequently enhanced the sensor performance of SnO₂ nanostructures. In our previous study, we found that the ethanol sensor response was greatly enhanced (by approximately 13 times) after SnO₂ was doped with 5 mol% Ni.¹⁶ It was proposed that the thickness of charge depletion layer and the presence of oxygen vacancies mainly contributed to the high sensor response.

Our literature search shows that there are not many comparative studies on ethanol gas sensing properties of pure, transition metal and noble metal-doped SnO₂ being reported. Furthermore, it can be difficult comparing the gas sensing properties between numerous research works since the synthesis routes and reaction conditions are different. Hence, in this study, we prepared pure SnO₂, Ni and Pd-doped SnO₂ nanorods by using a facile hydrothermal method. A comparative study was carried out exploring the role of transition metal dopants and noble metal dopants in promoting the ethanol gas sensor performance.

2. EXPERIMENTAL

2.1 Materials

All chemicals used in this study were of analytical grade without any further purification. Tin(IV) chloride pentahydrate, SnCl₄·5H₂O (98%), was obtained from Sigma Aldrich, United States. Nickel chloride hexahydrate, NiCl₂·6H₂O was purchased from Hamburg Chemical GmbH, Germany and palladium chloride, PdCl₂ was obtained from QRec. Chemical Co. Ltd, Thailand. Sodium hydroxide, NaOH and absolute ethanol, C₂H₅OH were procured from QRec Asia Sdn. Bhd., Malaysia.

2.2 Synthesis of SnO₂ Nanorods

The hydrothermal method for synthesis, pure and Ni-doped SnO₂ (Ni:SnO₂) nanorods had been reported in previous works.^{16,17} In brief, the precursor, including SnCl₄·5H₂O (4.8 mmol), and a calculated amount of NiCl₂·6H₂O (5 mol% Ni) and PdCl₂ (5 mol% Pd) were dissolved in 30 ml of an absolute ethanol-distilled water solvent (1:1 v/v) separately, with vigorous stirring to obtain a homogeneous solution. The pH of the solution was then adjusted to pH 13 by adding an equal volume of 6 M NaOH solution and absolute ethanol, simultaneously. The final volume of the reaction mixture was filled to 40 ml by adding ethanol-distilled water (1:1 v/v) mixture and was then transferred to a 50 ml Teflon-lined stainless-steel autoclave, sealed and heated at 180°C for 15 h. The product was centrifuged and

repeatedly washed with distilled water and ethanol, and later oven-dried at 55°C overnight. The pure SnO₂ sample was prepared as per the previously-mentioned process, except that heat treatment was carried out for 24 h without dopant.

2.3 Sample Characterisations

The crystal structure of the samples was determined by XRD (PW 3040/60 X'PERT PRO, PANalytical, Malvern, United Kingdom) using Cu K α radiation with a scanning step size of 0.0340°. The structural parameters were calculated by applying Rietveld analysis (semi-automatic mode) using the PANalytical X'Pert Highscore Plus (version 2.2) software. The surface composition was investigated using X-ray photoelectron spectroscopy (XPS, Axia Ultra DLDXPS, Kratos, Manchester, United Kingdom) with a monochromatic Al K α X-ray source (1486.6 eV of photons) and background pressure of 10⁻⁷ Pa. All the reported binding energy (BE) data were calibrated using the C 1s line at 284.6 eV. CASAXPS (version 2.3.17) software was used for analysing the XPS spectra. A GL (30) Gaussian (70%)-Lorentzian (30%) profile and a standard Shirley background were applied for fitting the components. The morphologies of the samples were examined by FESEM (LEO 1525, 30 kV, New York, United States) and high-resolution transmission electron microscopy (HRTEM, TECNAI G2 20 S-TWIN, FEI, China) at 200 kV. For FESEM characterisation, the as-synthesised SnO₂ samples were sputtered on aluminium stub which was covered with carbon tape. The samples were then coated with a thin layer of gold to increase the electron conduction which subsequently improved the quality of images. Meanwhile, for HRTEM analysis, the as-synthesised SnO₂ powder samples were dispersed in absolute ethanol and ultrasonicated for 30 min. The dispersion was then dropped on carbon-copper grids.

2.4 Sensor Preparation and Ethanol Gas Sensing Measurement

Details of the sensor preparation and the configuration of custom-built gas sensing measurement instrumentation can be found in our previous work.¹⁶ In brief, a proper amount of as-synthesised SnO₂ samples were mixed in sensor ink separately to form a slurry.¹⁸ Subsequently, the slurry was coated onto an Au-interdigitated alumina substrate covering a dimension of 5 mm × 5 mm (Case: Western Reserve University, Cleveland, United States). In order to stabilise the sensor material, the substrates were heat-treated at 450°C in argon gas flow prior to use. For the purpose of determining the optimum operating temperature, gas sensing measurement was performed at 200°C–450°C using the pure SnO₂ nanorods sensor, with 1000 ppm ethanol C₂H₅OH in nitrogen (N₂) gas environment. The total flow rate was maintained at 200 sccm throughout the experiment. It was found that at 450°C,

the pure SnO₂ nanorods sensor demonstrated good sensing properties. Further gas sensing measurements were recorded at 450°C. The sensor response at different concentrations (50–1000 ppm) was investigated by diluting 1000 ppm ethanol gas with nitrogen gas. The response to ethanol gas is defined as R_0/R_g where R_0 and R_g are the resistances of SnO₂ sensor materials in nitrogen gas and in C₂H₅OH gas, respectively. The response time is expressed as the duration taken by the sensor to achieve 90% of the total resistance changes upon the adsorption of C₂H₅OH gas. The recovery time is defined as the duration taken by the sensor to achieve 90% of total resistance changes upon the removal of C₂H₅OH gas.

3. RESULTS AND DISCUSSION

3.1 Compositional and Morphological Analysis

The XRD patterns of pure SnO₂, Ni:SnO₂ and Pd:SnO₂ nanorods samples are presented in Figure 1. The unit cell parameters were calculated by means of the Rietveld refinement which are listed in Table 1. All the diffraction peaks can be indexed as rutile tetragonal phase SnO₂ (SG, $P4_2/mnm$) (ICSD no. 98-005-7394, $a = b = 4.7380$ Å and $c = 3.1870$ Å). No trace of other phases (e.g., SnO, PdO, Pd, Ni, NiO, etc.) were detected. It was found that the addition of dopants (5 mol% Pd and 5 mol% Ni) in SnO₂ crystal structures induced a broadening and an intensity alteration of peaks, indicating a reduction in particle size and crystallinity.¹⁹ The Rietveld refinement showed that the lattice parameters of pure SnO₂ nanorods were $a = 4.7503$ Å and $c = 3.1838$ Å, whereas, slight changes in lattice parameters and crystallite size were recorded after doping with Ni and Pd. This phenomenon could be due to the substitution of Sn⁴⁺ ions with Ni²⁺ and Pd²⁺ ions.²⁰ It is worth noting that the lattice parameters and crystallite size of Pd:SnO₂ is slightly larger than Ni:SnO₂, which is most likely due to the ionic radii of Pd²⁺ ion (86 pm) which is larger than Ni²⁺ (69 pm).^{21,22}

Hence, the substitution of Ni²⁺ in SnO₂ lattice structure leads to more significant variations in lattice parameters and crystallite size compared to Pd doping. Moreover, as a dopant, Ni is known to inhibit the growth of crystals.¹³ The high intensity peaks of (110), (101) and (211) indicate the preferential crystal planes of nanorods.²³

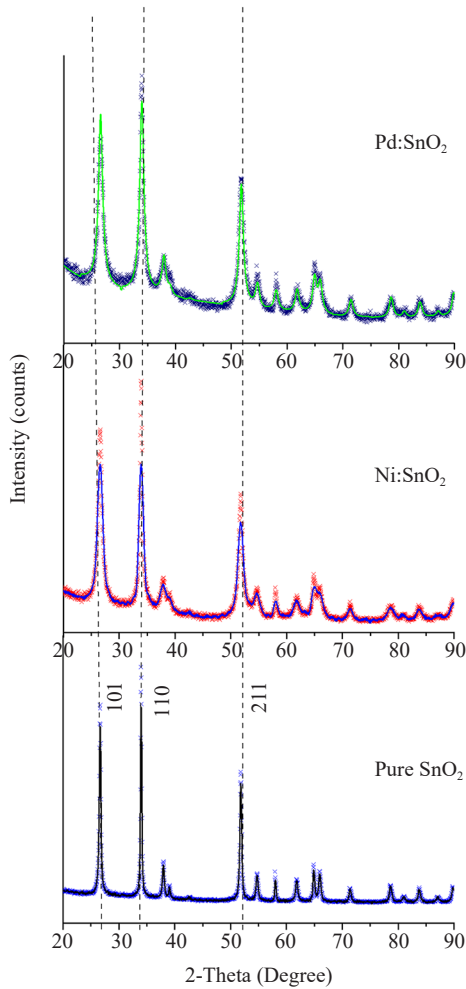


Figure 1: XRD patterns of as-synthesised SnO_2 samples. The experimental data and Rietveld refinement fitting are represented with symbols and solid lines, respectively (ref. ICSD no. 98-005-7394).

Table 1: The lattice parameters and the mean crystallite size calculated using Rietveld refinement.

| Samples | Lattice parameters (\AA) | | Mean crystallite size, nm |
|---------------------|-------------------------------------|--------|---------------------------|
| | a | c | |
| Pure SnO_2 | 4.7503 | 3.1838 | 28.3 |
| Ni: SnO_2 | 4.7473 | 3.1800 | 6.2 |
| Pd: SnO_2 | 4.7481 | 3.1820 | 7.3 |

The morphology and size of as-synthesised SnO_2 nanorod samples were characterised by both FESEM and HRTEM. The FESEM images (Figure 2) confirmed the formation of nanorods in all three SnO_2 samples. From the results, it can be seen clearly that the nanorods grew into closely packed flower-like bunches. It is worth noting that even in the absence of dopants (pure SnO_2), similar morphology was obtained. This observation led to the conclusion that in this study, the shape of the particles was not influenced by the dopants. However, evidence shows that higher amount of dopants could act as a structure-directing agent in metal oxide nanostructures.^{5,24}

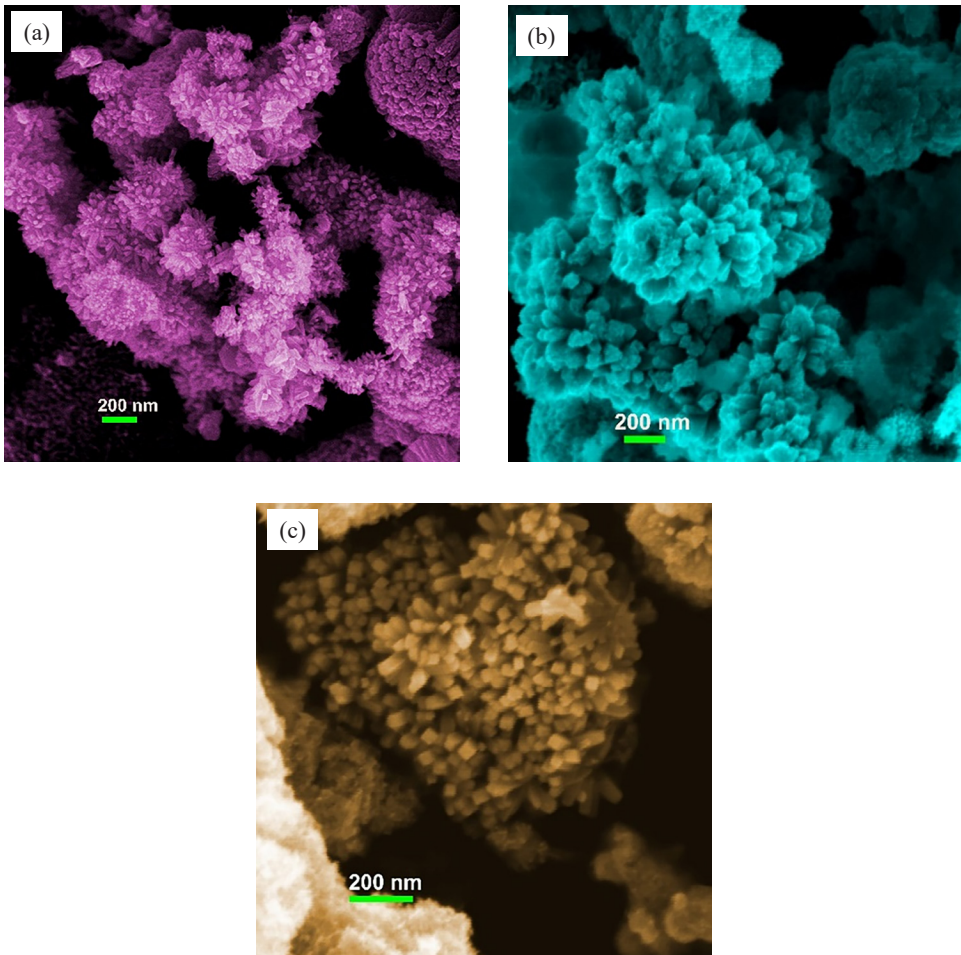


Figure 2: FESEM images of as-synthesised samples for (a) pure SnO_2 , (b) Ni: SnO_2 nanorods, and (c) Pd: SnO_2 nanorods.

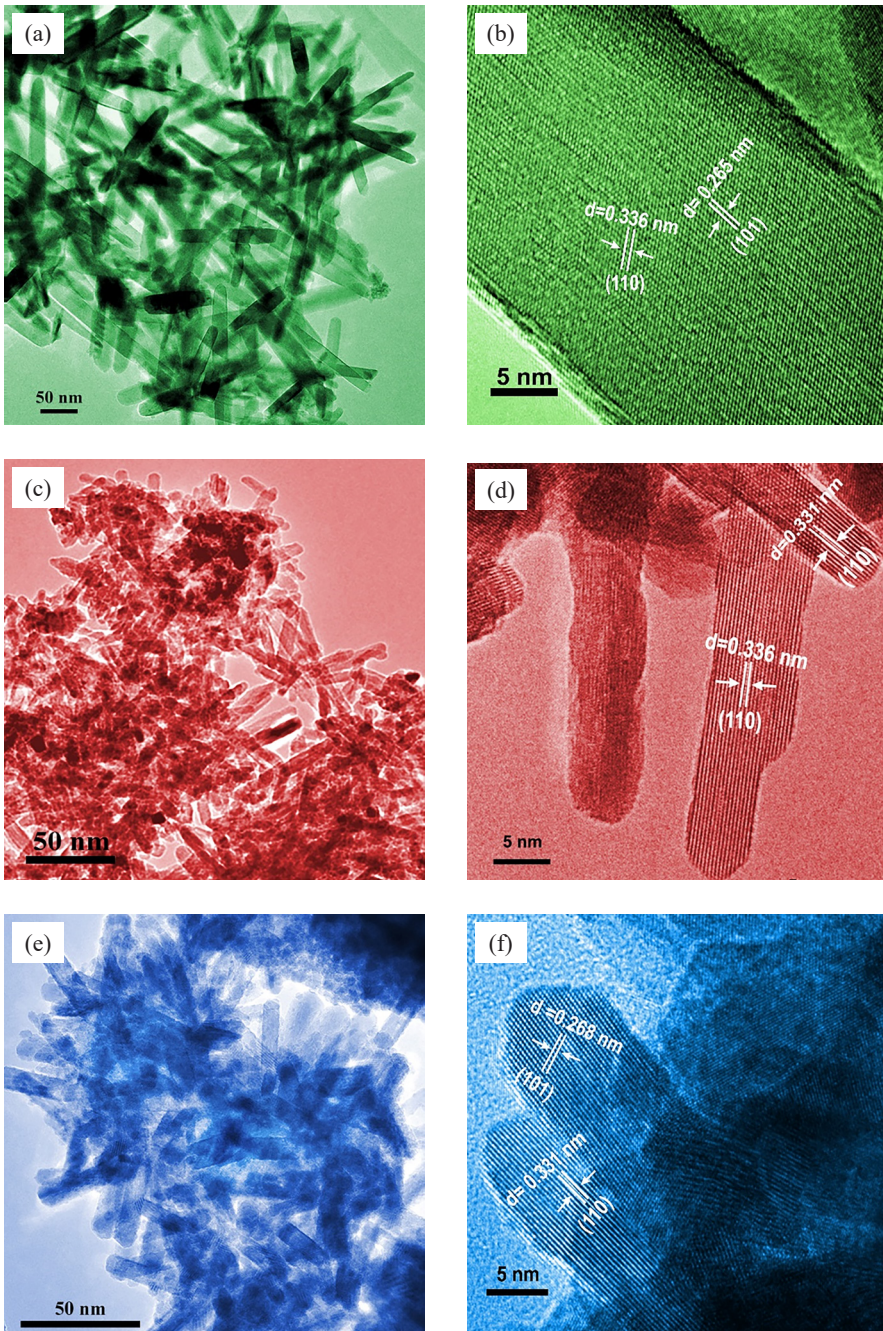


Figure 3: HRTEM images of: (a and b) pure SnO_2 , (c and d) Ni:SnO_2 , and (e and f) Pd:SnO_2 nanorods, respectively.

Further morphology characterisation was studied using HRTEM analysis. Figure 3(a, c and e) exhibits the morphologies of as-synthesised SnO₂ nanorods. Meanwhile, Figure 3(b, d to f) shows the enlarged images of all the samples, where the lattice fringes can be observed clearly. The nanorods formed in pure SnO₂ typically had an average diameter of ~25 nm. Meanwhile, the average diameter of nanorods in Ni:SnO₂ and Pd:SnO₂ were ~6 nm and ~10 nm, respectively. This finding is supported by XRD data (broadening of peaks), where the particle size was reduced in Ni:SnO₂ and Pd:SnO₂ nanorods samples. On the other hand, the lattice fringes of all the samples confirmed the single crystal nature of the SnO₂ nanorods.²⁵ The lattice spaces in pure SnO₂ (Figure 3(b)) were ~0.336 nm and ~0.265 nm, which attributed to (110) and (101) planes of the tetragonal rutile crystal structure. Meanwhile, for Ni:SnO₂ nanorods, as shown in Figure 3(d), the lattice fringe were found to be ~0.336 nm and ~0.331 nm, which were assigned to plane (110) tetragonal rutile indicating that the preferential growth direction was [001].²⁶ Likewise, lattice spaces for Pd:SnO₂, shown in Figure 3(f) were identified as ~0.331 nm and ~0.268 nm which corresponded to plane (110) as well as (101) respectively. This result is in good agreement with XRD patterns where the planes (110) and (101) were among the strongest peaks recorded for all the three SnO₂ samples.

The chemical composition and chemical state of the as-synthesised SnO₂ samples were investigated using XPS. In our previous paper, we discussed in detail the XPS result of pure SnO₂ and Ni:SnO₂ nanorods samples.¹⁶ In brief, XPS results of pure SnO₂ and Ni:SnO₂ nanorods samples confirmed the formation of SnO₂. The presence of O 1s lattice oxygen (O-Sn-O) peak was detected, and another peak corresponding to oxygen ions in deficient regions were identified in both pure and Ni doped SnO₂ samples, respectively. An additional O 1s peak, which ascribed to surface absorbed oxygen ions was identified in Ni:SnO₂. Also, no other peaks such as Ni, Ni₂O₃ or NiO were found in the Ni:SnO₂ sample.

In this current work, we only focused on the XPS result of Pd:SnO₂. Figure 4 exhibits the XPS high resolution spectra of the Pd:SnO₂ sample. Unlike the pure SnO₂ and Ni:SnO₂ nanorod samples, two types of Sn species were identified in Pd:SnO₂. The main peaks were assigned as Sn⁴⁺ 3d_{5/2} (486.2 eV) and Sn⁴⁺ 3d_{3/2} (494.6 eV), which confirmed the presence of SnO₂.²⁷ Also, the peaks of Sn²⁺ 3d_{5/2} and Sn²⁺ 3d_{3/2} were detected in Pd:SnO₂ samples, suggesting that Sn⁴⁺ ions were partially reduced to Sn²⁺ during the doping process. This observation is similar to a previous study by Aragón et al.²⁰ On the other hand, the region of O 1s in Pd:SnO₂ could be de-convoluted into three different oxygen peaks. The higher binding energy O 1s peak was ascribed to , O[•] and OH⁻ at oxygen deficient regions

which played an important role in influencing gas sensing properties.¹³ The peak at the binding energy of 529.9 eV was assigned to lattice oxygen O^{2-} in the O-Sn-O bond. Another peak was recorded at the higher binding energy of 531.1 eV, which corresponded to the coordination of oxygen in Sn-O-Pd.²⁴ This result is supported by the Pd^{2+} 3d peaks as shown in Figure 4(c). The doublet peaks at 342.3 eV and 336.5 eV were binding energies of Pd^{2+} $3d_{3/2}$ and Pd^{2+} $3d_{5/2}$, respectively, which suggests that Pd-O is bonded in Sn-O-Pd.²⁸ Unlike Ni:SnO₂, metallic Pd^0 peaks were identified in Pd:SnO₂ sample. Based on the above mentioned data, the Pd:SnO₂ nanorods sample could contain Pd clusters such as Pd and PdO as surface species.

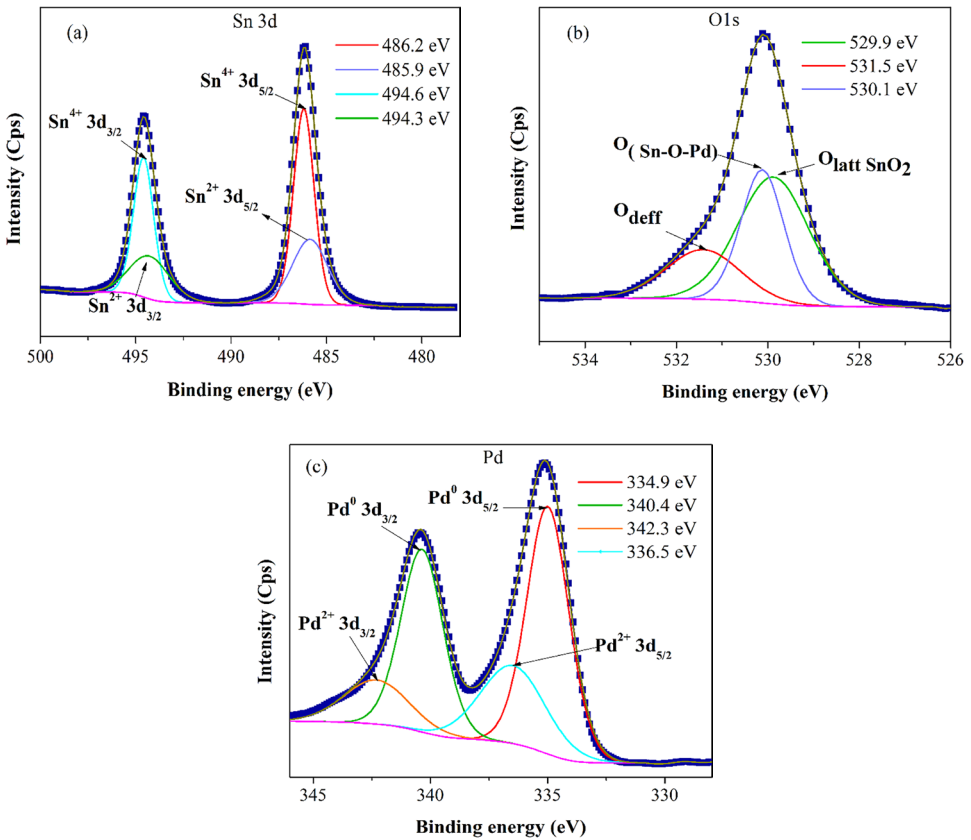


Figure 4: The XPS spectra of Pd:SnO₂ nanorod sample.

3.2 Gas Sensing Measurement

In order to evaluate the gas sensing properties, all the as-synthesised SnO₂ nanorods sensors were first tested with 1000 ppm ethanol (C₂H₅OH) gas at an optimum operating temperature of 450°C in nitrogen gas flow. Figure 5 presents responses to 1000 ppm of C₂H₅OH gas for the pure SnO₂, Ni:SnO₂ and Pd:SnO₂ nanorods sensors. From the results obtained, it can be seen that pure SnO₂ nanorods revealed a very low sensor response, ($R_0/R_g \sim 1.1 \times 10^3$). However, the response recorded a drastic increase after the doping process. The response values of Ni:SnO₂ and Pd:SnO₂ sensors were $R_0/R_g \sim 1.4 \times 10^4$ and $R_0/R_g \sim 1.7 \times 10^4$, respectively.

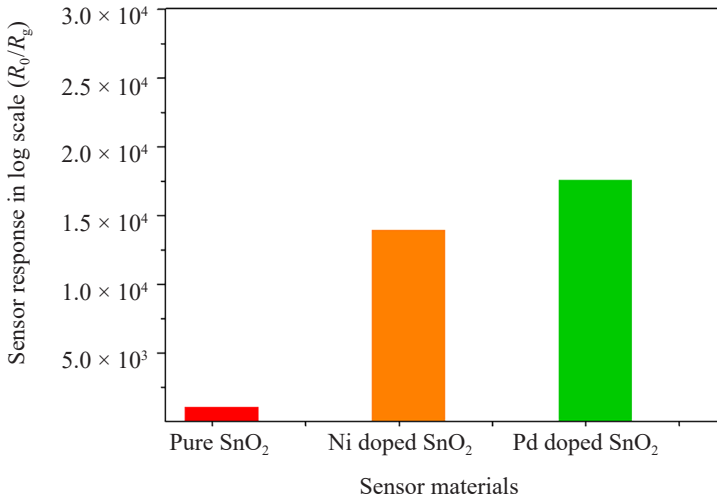


Figure 5: As-synthesised SnO₂ nanorods sensors response to 1000 ppm C₂H₅OH/N₂ gas at operating temperature of 450°C.

Figure 6 shows the resistance curves for as-synthesised SnO₂ nanorod sensors. It was observed that the initial resistances of Pd:SnO₂ was much higher than pure SnO₂ and Ni:SnO₂ nanorods sensors. A similar result was also observed by Chen et al. and Fedorenko et al.^{28,29} It was explained that the presence of two forms of Pd clusters (Pd and PdO) in the SnO₂ sensor system influenced the initial resistance. This is because more chemisorption of oxygen takes place at the common edge between Pd/PdO and SnO₂, which eventually increased the initial resistance of the sensor. All the samples revealed the same response time, 40 s, but had different recovery times. It is worth noting that the recovery time of Ni:SnO₂ was improved compared to pure SnO₂, where the recovery time was found to be considerably longer. On the contrary, Pd:SnO₂ showed almost 100% recovery in 12 min. Thus, Pd:SnO₂ shows a high sensor response with fast recovery as well as response time.

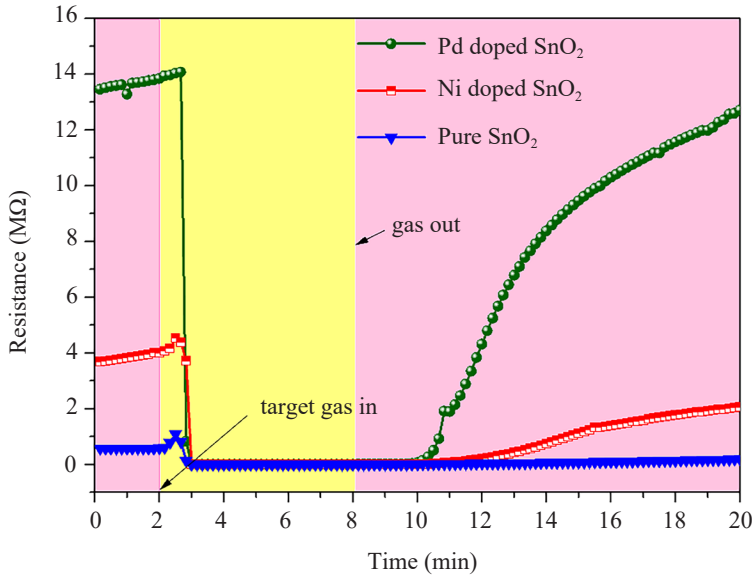


Figure 6: The resistance curves of as-synthesised SnO₂ nanorod sensor.

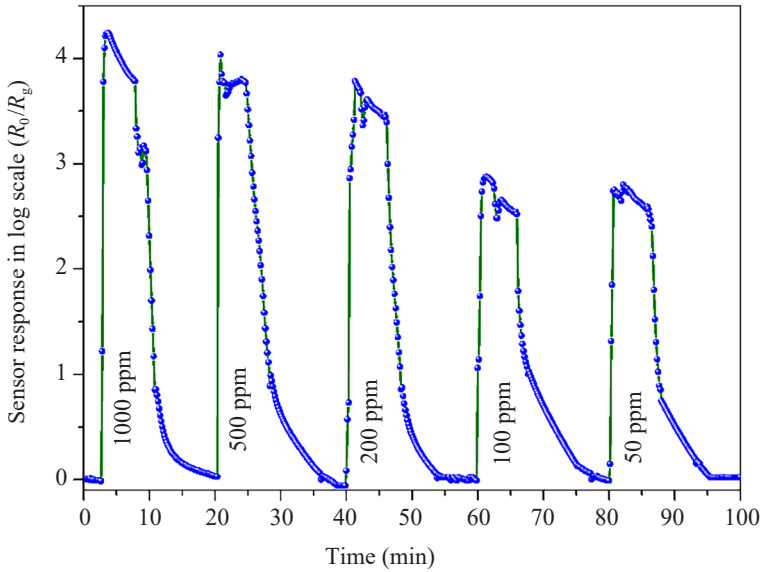


Figure 7: Continuous response-recovery curves of Pd:SnO₂ nanorod sensor for various C₂H₅OH gas concentrations at 450°C.

Upon further investigation, the Pd:SnO₂ nanorod sensor was tested with different C₂H₅OH gas concentrations (50 ppm, 100 ppm, 200 ppm, 500 ppm and 1000 ppm). Figure 7 shows the real-time response curve of Pd:SnO₂ nanorods sensor to C₂H₅OH. It was observed that the responses gradually increased from 6.4×10^2 , 7.6×10^2 , 6.9×10^3 , 1.0×10^4 and 1.7×10^4 with the increase of C₂H₅OH gas concentration of 50 ppm, 100 ppm, 200 ppm, 500 ppm and 1000 ppm, respectively. The response time reduced from 40 s to 30 s as the concentration decreased from 1000 ppm to 50 ppm. Similarly, the recovery time also reduced from 12 min to 8 min. Meanwhile, Figure 8 shows that the linearity of the Pd:SnO₂ nanorods sensor performed better at higher concentration range (200–1000 ppm) of C₂H₅OH gas than the lower concentration range.

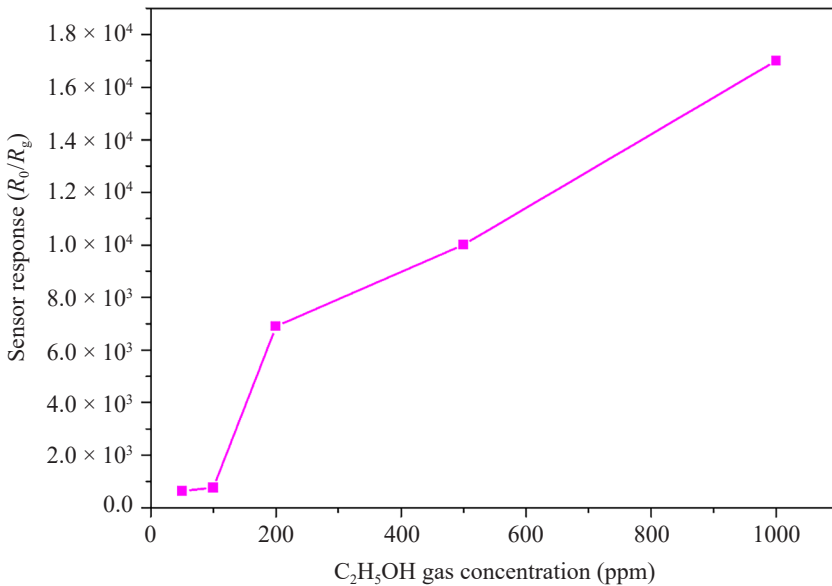


Figure 8: Sensor response of Pd:SnO₂ nanorods for different C₂H₅OH gas concentrations (50–1000 ppm) at 450°C.

3.3 Ethanol Gas Sensor Mechanism

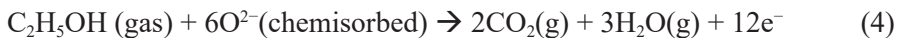
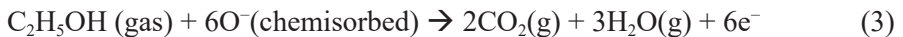
In general, gas sensor response is defined as the transfer of electrons on the sensor material when gas sensing reaction takes place.³¹ In this study, the Pd:SnO₂ nanorod sensor showed high C₂H₅OH sensing response and fast recovery time. It is postulated that the introduction of Pd into SnO₂ nanorods can bring several changes in physical and chemical properties which lead to the enhancement of gas sensor properties. Firstly, the interface between two forms of Pd/PdO and SnO₂ remarkably increased the chemisorption of oxygen.^{10,30} It is worth noting

that the initial resistance, R_o , greatly depends on the chemisorbed oxygen content. Secondly, the 1-D SnO₂ nanorods with considerably smaller sizes (~10 nm) could provide a large surface-to-volume ratio which contributed to more active sites to react. Thirdly, Pd dopants can act as a catalytic site in facilitating oxidation reaction. Lastly, oxygen vacancies at oxygen deficient regions also play a vital effect on the sensor properties of Pd:SnO₂.

Based on the results obtained, we propose a mechanism for C₂H₅OH gas sensing in the Pd:SnO₂ system. At ambient temperature, oxygen molecules in the air adsorbed at the interface of active additives and SnO₂ (Equation 1). At temperatures of 150°C–300°C, oxygen molecules ionised into oxygen species, for instance O₂⁻, O⁻ and O²⁻ ions, by trapping the electrons from conductive bands and subsequently forming negatively-charged surface potential (Equation 2).³² As the operating temperature increased to 450°C, atomic ion species (O⁻ and O²⁻) dominated.³² Thus, the near surface layer of the sensor material became depleted by electrons. This eventually impeded the transfer of electron in the sensor material. As a result, the initial resistance increased drastically. Moreover, the presence of oxygen vacancies in oxygen deficient regions also partly contributed to the amount of surface oxygen ions. When the sensor was exposed to C₂H₅OH gas, the ethanol gas reacted with the chemisorbed oxygen ion species on the active sites and eventually transferred back the electrons which in turn reduced the depletion layer (Equations 3 and 4). Hence, a decrease in resistance was recorded. It should be noted that the high sensor response not only depends on the amount of chemisorbed oxygen, but also on the temperature where the high catalytic activity was obtained at 450°C.¹⁰ During the recovery process, the sensor returned to its initial condition by trapping the electrons again.³³



where $\alpha = 1$ for atomic oxygen, $\alpha = 2$ for oxygen molecule, $\beta = 1$ for singly ionised, and $\beta = 2$ for doubly ionised.



4. CONCLUSION

The pure SnO₂, Ni:SnO₂ and Pd:SnO₂ nanorods were successfully synthesised through a template-free hydrothermal method. The diameter of nanorods were found to be reduced after the doping process. The XPS result of Pd:SnO₂ revealed that there were more than one Pd clusters (Pd and PdO) formed during the hydrothermal synthesis. The gas sensing measurement showed that the Pd:SnO₂ nanorod sensor drastically improved the C₂H₅OH sensor response and recovery time compared to pure SnO₂ and Ni:SnO₂ nanorods sensors. Overall, we conclude that the chemical state of Pd, the oxygen vacancies and the 1-D nanostructure of Pd:SnO₂ are mainly responsible for the high C₂H₅OH gas sensing response.

5. ACKNOWLEDGEMENTS

The authors gratefully acknowledge the Department of Research and Innovation, Universiti Sains Malaysia (USM) for financial assistance provided for this research under the Bridging Fund (304.PKIMIA.6316030).

6. REFERENCES

1. Seiyama, T. et al. (1962). A new detector for gaseous components using semiconductive thin films. *Anal. Chem.*, 34(11), 1502–1503, <https://doi.org/10.1021/ac60191a001>.
2. Zeng, W. et al. (2014). Hydrothermal synthesis of hierarchical flower-like SnO₂ nanostructures with enhanced ethanol gas sensing properties. *Mater. Res. Bull.*, 57, 91–96, <https://doi.org/10.1016/J.MATERRESBULL.2014.05.019>.
3. Cao, S. et al. (2015). Hydrothermal synthesis of SnO₂ nanocubes and nanospheres and their gas sensing properties. *J. Mater. Sci. Mater. Electron.*, 26(5), 2871–2878, <https://doi.org/10.1007/s10854-015-2771-3>.
4. Comini, E. et al. (2002). Stable and highly sensitive gas sensors based on semiconducting oxide nanobelts. *Appl. Phys. Lett.*, 81(10), 1869–1871, <https://doi.org/10.1063/1.1504867>.
5. Yang, F. & Guo, Z. (2015). Comparison of the enhanced gas sensing properties of tin dioxide samples doped with different catalytic transition elements. *J. Coll. Interf. Sci.*, 448, 265–274, <https://doi.org/10.1016/j.jcis.2015.02.045>.
6. Sun, Y. F. et al. (2012). Metal oxide nanostructures and their gas sensing properties: A review. *Sens.*, 12(12), 2610–2631, <https://doi.org/10.3390/s120302610>.
7. Li, Y. et al. (2016). Highly sensitive ethanol sensor based on au-decorated SnO₂ nanoparticles synthesised through precipitation and microwave irradiation. *J. Electron. Mater.*, 45(6), 3149–3156, <https://doi.org/10.1007/s11664-016-4438-0>.

8. Sokovykh, E. V. et al. (2017). Influence of conditions of Pd/SnO₂ nanomaterial formation on properties of hydrogen sensors. *Nanos. Res. Lett.*, 12(1), 383, <https://doi.org/10.1186/s11671-017-2152-3>.
9. Kappler, J. N. et al. (1998). Correlation between XPS, Raman and TEM measurements and the gas sensitivity of Pt and Pd doped SnO₂ based gas sensors. *Fres. J. Anal. Chem.*, 361(2), 110–114, <https://doi.org/10.1007/s002160050844>.
10. Lee, Y. C. et al. (2008). Semiconductor gas sensor based on pd-doped SnO₂ nanorod thin films. *Sens. Actuat. B Chem.*, 132(1), 239–242, <https://doi.org/10.1016/J.SNB.2008.01.028>.
11. Ivanov, P. et al. (2004). Development of high sensitivity ethanol gas sensors based on Pt-doped SnO₂ Surfaces. *Sens. Actuat. B Chem.*, 99(2–3), 201–206, <https://doi.org/10.1016/j.cap.2013.05.016>.
12. Lin, Z. et al. (2017). The effect of Ni doping concentration on the gas sensing properties of Ni doped SnO₂. *Sens. Actuat. B*, 239, 501–510, <https://doi.org/10.1016/j.snb.2016.08.053>.
13. Parthibavarman, M., Renganathan, B. & Sastikumar, D. (2013). Development of high sensitivity ethanol gas sensor based on Co-doped SnO₂ nanoparticles by microwave irradiation technique. *Curr. Appl. Phys.*, 13(7), 1537–1544, <https://doi.org/10.1016/j.cap.2013.05.016>.
14. Galatsis, K. et al. (2003). P- and N-type Fe-doped SnO₂ gas sensors fabricated by the mechanochemical processing technique. *Sens. Actuat. B Chem.*, 93(1–3), 562–565, [https://doi.org/10.1016/S0925-4005\(03\)00233-8](https://doi.org/10.1016/S0925-4005(03)00233-8).
15. Wu, N. L., Wang, S. Y. & Rusakova, I. A. (1999). Inhibition of crystallite growth in the sol-gel synthesis of nanocrystalline metal oxides. *Sci.*, 285(5432), 1375–1377, <https://doi.org/10.1126/science.285.5432.1375>.
16. Inderan, V. et al. (2017). Study of structural properties and defects of Ni-doped SnO₂ nanorods as ethanol gas sensors. *Nanotechnol.*, 28(26), 265702, <https://doi.org/10.1088/1361-6528/aa731c>.
17. Inderan, V. (2015). Synthesis and characterisations of SnO₂ nanorods via low temperature hydrothermal method. *Superlatt. Microst.*, 88, 396–402, <https://doi.org/10.1016/j.spmi.2015.09.031>.
18. Arafat, M. M., Haseeb, A. S. M. A. & Akbar, S. A. A. (2014). Selective ultrahigh responding high temperature ethanol sensor using TiO₂ nanoparticles. *Sens. (Basel)*, 14(8), 13613–13627, <https://doi.org/10.3390/s140813613>.
19. Yogamalar, R. et al. (2010). Gas-sensing properties of needle-shaped Ni-doped SnO₂ nanocrystals prepared by a simple sol-gel chemical precipitation method. *Chem. Asian J.*, 5(11), 2379–2385, <https://doi.org/10.1002/asia.201000358>.
20. Aragón, F. H. et al. (2016). Fe doping effect on the structural, magnetic and surface properties of SnO₂ nanoparticles prepared by a polymer precursor method. *J. Phys. D Appl. Phys.*, 49(15), 155002, <https://doi.org/10.1088/0022-3727/49/15/155002>.
21. Cai, X. et al. (2013). Structural and photocatalytic properties of nickel-doped zinc oxide powders with variable dopant contents. *J. Phys. Chem. Solids.*, 74(9), 1196–1203, <https://doi.org/10.1016/j.jpcs.2013.03.016>.

22. Huang, S. et al. (2016). enhanced photocatalytic activity of TiO₂ activated by doping Zr and modifying Pd. *RSC Adv.*, 6(36), 29950–29957, <https://doi.org/10.1039/C6RA03275C>.
23. Vomáčka, P. et al. (2016). Shape-controlled synthesis of Sn-doped CuO nanoparticles for catalytic degradation of Rhodamine B. *J. Coll. Inter. Sci.*, 481, 28–38, <https://doi.org/10.1016/j.jcis.2016.07.026>
24. Jia, T. et al. (2009) Synthesis, characterization, and photocatalytic activity of Zn-doped SnO₂ hierarchical architectures assembled by nanocones. *J. Phys. Chem. C*, 113, 9071–9077, <https://doi.org/10.1021/jp9021272>.
25. Sun, P. et al. (2011). One-step synthesis and gas sensing characteristics of hierarchical SnO₂ nanorods modified by Pd loading. *Sens. Actuat. B Chem.*, 160(1), 244–250, <https://doi.org/10.1016/j.snb.2011.07.043>.
26. Birkel, A. et al. (2010). Interaction of alkaline metal cations with oxidic surfaces: effect on the morphology of SnO₂ nanoparticles. *Langmuir*, 26(5), 3590–3595, <https://doi.org/10.1021/la902994r>.
27. Liang, Y. & Fang, B. (2013). Hydrothermal synthesis of SnO₂ nanorods: Morphology dependence, growth mechanism and surface properties. *Mater. Res. Bull.*, 48(10), 4118–4124, <https://doi.org/10.1016/J.MATERRESBULL.2013.06.040>.
28. Chen, Y. Qin, H. & Hu, J. (2018). Applied surface science Co sensing properties and mechanism of Pd doped SnO₂ thick-films. *Appl. Surf. Sci.*, 428, 207–217, <https://doi.org/10.1016/j.apsusc.2017.08.205>.
29. Fedorenko, G. et al. (2017). Semiconductor gas sensors based on Pd/SnO₂ nanomaterials for methane detection in air. *Nanos. Res. Lett.*, 12(329), 1–9, <https://doi.org/10.1186/s11671-017-2102-0>.
30. Oleksenko, L. P. et al. (2014). Study of influence of palladium additives in nanosized tin dioxide on sensitivity of adsorption semiconductor sensors to hydrogen. *Sens. Actuat. B. Chem.*, 196, 298–305, <https://doi.org/10.1016/j.snb.2014.02.019>.
31. Das, S. & Jayaraman, V. (2014). A comprehensive review on structures and gas sensors. *Prog. Mater. Sci.*, 66, 112–255, <https://doi.org/10.1016/j.pmatsci.2014.06.003>.
32. Barsan, N. & Weimar, U. (2001). Conduction model of metal oxide gas sensors. *J. Electrocer.*, 7, 143–167, <https://doi.org/10.1023/A:1014405811371>.
33. Wu, Q., Li, J. & Sun, S. (2010). Nano SnO₂ gas sensors. *Curr. Nanosci.*, 2, 525–538, <https://doi.org/10.2174/157341310797574934>.